Estimating Central Pressures of Oceanic Midlatitude Cyclones

R. A. BROWN AND LIXIN ZENG

Department of Atmospheric Sciences, University of Washington, Seattle, Washington

(Manuscript received 20 September 1993, in final form 1 January 1994)

ABSTRACT

A method of determining surface pressures in oceanic storm systems using *ERS-1* scatterometer data is employed to determine the lowest pressures in 25 storms. This method uses the surface winds as a lower boundary condition on a planetary boundary layer model to determine gradient winds and, thereby, pressure gradients. An optimization scheme referenced to a pressure outside the storm provides a pressure field and an estimate of the low pressure. The values are compared to ECMWF analyses in each case; there is good agreement, with some expected differences.

1. Introduction

The central pressure of a cyclone is one measure of the cyclone's intensity. It is also difficult to obtain from measurements. Oceanic surface observations are sparse at best and are limited mainly to heavily traveled shipping lanes. Even these observations are often sporadic, particularly in storms—sufficiently erratic that if a measurement is unusual, it is discarded. Some are obviously spurious, like the ship report from Kansas, but other "outliers" are likely to be the singularly unusual pressure without supporting data. However, such a measurement might be the only one that would indicate a quickly changing low center. The situation is worse for night reports and abysmal for areas outside shipping lanes. As a result, there are seldom good storm low pressures for initializing the numerical analyses.

Meteorological center numerical analyses frequently have difficulty identifying the intense storms due to resolution problems. A finer grid generally results in deeper lows for the midlatitude storms. Current analyses are too high by several millibars in some storms. Although the situation can be improved by ad hoc surface pressure bogusing schemes based on satellite cloud images (e.g., Smigielski and Mogil 1991), these procedures inevitably have their limitations.

Efforts to improve analyses of storms' intensities have focused on satellite visual and IR observations. Initially, schematics of cloud formations were correlated with surface lows in studies by Anderson et al. (1973), Guymer (1978), Junker and Haller (1980), and Smigielski and Mogil (1991). Through these efforts, several simple and tenuous characteristics of developing lows were associated with cloud development:

1) normal extratropical cyclones develop from wave to maturity in about 72 h;
2) some cyclones develop in less than 48 h;
3) if positive vorticity advection is present, often indicated by a comma cloud in the lee of the front, the low can be reinforced; and
4) baroclinic zones, defined by certain broad bands of clouds in midlatitude storms, are related to circulation and hence central pressure of the storm.

Particular cloud pictures are correlated to the state of storm development and thereby to pressure tendency. Thus, certain cloud patterns would suggest deepening or filling of the lows. This scheme has an accuracy of about ±5 mb and apparently represents an improvement over National Meteorological Center (NMC) analyses from surface data alone (Smigielski and Mogil 1991). We are not aware of any such schemes in the European Centre for Medium-Range Weather Forecasts (ECMWF) analysis. We found good agreement between ECMWF and NMC in the NMC fine-mesh region. Since this is a limited region, we have compared *ERS-1* scatterometer/planetary boundary layer (or scat/PBL) pressures globally to ECMWF analyses.

2. Scatterometer-derived surface pressures

The method used here is to employ *ERS-1* scatterometer winds as a lower boundary condition on a PBL model. The model yields surface geostrophic or gradient flows, which correspond to pressure gradients. A single ECMWF surface pressure point at a uniform region removed from the storm center is sufficient to provide magnitudes. One can obtain the pressure field by either of two methods. In the first, integration proceeds from a reference pressure in the uniform region to provide a minimum pressure at the low center. In

Corresponding author address: R. A. Brown, Department of Atmospheric Sciences, University of Washington, Seattle, WA 98195.

the second, an optimization scheme relates the pressure field to the specified point or region. In this paper, we use the latter scheme.

The winds from *ERS-1* were obtained from the National Aeronautics and Space Administration/Jet Propulsion Laboratory (NASA/JPL) Freilich–Dunbar (1992) algorithm. This is a statistical correlation between radar backscatter coefficient σ_0 and the NMC global analyzed surface wind. These winds are generally equal to or less than the true winds (Foster and Brown 1994). Thus, our results are not so much an independent quantitative measure of the scat/PBL method as a demonstration of the ability to define storm details. The *ERS-1* data center provides winds using another algorithm. We will investigate the differences in the pressure fields using these winds in future studies.

3. The inverse PBL model

The University of Washington (UW) PBL model is a 1D similarity model that accounts for stratification, variable surface roughness, thermal wind, and organized large eddy effects. This is an analytic solution of the matching of a quasi-nonlinear Ekman solution to a log-layer solution. The latter is corrected for interfacial layer effects according to Liu et al. (1979). The ratio of characteristic wind speeds in the two layers (u^*/G is the geostrophic drag coefficient) is proportional to a single similarity parameter that is the ratio of the characteristic heights of the two layers, $h/\delta = \lambda$. For variable stratification, this parameter is approximately a constant, 0.15. This direct link with the similarity relation between surface winds and gradient winds thus requires no detailed calculations within the PBL. The version used in this study is the inverse of the UW two-layer similarity model described by Brown and Liu (1982) and Brown and Foster (1994).

The input to the inverse model is the surface wind field measured by a satellite scatterometer. The model then computes surface gradient winds and/or surface geostrophic winds. The corresponding pressure gradient is assumed to be impressed on the surface through the thin PBL. It can then be used to provide surface pressures. The model includes parameterizations for variable stratification in the two layers, variable surface roughness, and organized large eddy effects. A thermal wind correction is calculated. The initial procedure integrates from a known pressure throughout the field. This procedure is described in Brown and Levy (1986). However, when the wind field is significantly ageostrophic, another method is preferred. This takes advantage of the decomposition of the wind vector into divergent and nondivergent (geostrophic) parts.

When the geostrophic wind field is known, the pressure field can also be obtained by solving Poisson's equation with Neumann boundary conditions. However, the surface geostrophic wind computed from the inverse PBL model is usually not 100% geostrophic (or gradient), mainly because the input to the model, the scatterometer wind field, is sometimes noisy. A method for computing pressure from the "noisy" scatterometer-derived geostrophic winds must be employed. This approach is based on the fact that the surface geostrophic wind computed from the PBL model ($\mathbf{V}_{g1}$) is a good approximation of the true surface geostrophic wind. The model solves for a surface pressure such that the corresponding geostrophic wind $\mathbf{V}_g$ is as close to $\mathbf{V}_{g1}$ as possible in a global sense. When the field is represented on a discrete grid the problem becomes that of minimizing a cost function J defined by

$$J = \sum |\mathbf{V}_g - \mathbf{V}_{g1}|,$$

where the summation is done over all grid points N that have surface geostrophic wind either calculated by the PBL model or interpolated from neighboring points. The contribution to J from grid points where scatterometer-derived wind values are not available is excluded. Here $\mathbf{V}_g$ is obtained from the surface pressure by a finite-difference scheme. This is a minimization problem that involves solving an $N \times N$ linear system. A reference point for the pressure is required to determine the final value of the surface pressure. Details can be found in the appendix.

Since complete observations of surface air temperature and sea surface temperature are generally not available, neutral stratification and barotropic conditions have usually been assumed in this study. However, in some cases, the ECMWF model analyses of surface air temperature and sea surface temperature were used to investigate the sensitivity of the model results to PBL stratification and thermal wind. This was found to produce differences up to ±2 mb between the central pressures.

4. Analysis

Although the ECMWF and scat/PBL pressure fields were generally remarkably similar, some storms illustrated significant differences in the analyses. The reasons for differences could be 1) bad scatterometer winds, 2) a bad or inadequate PBL model, 3) inappropriate temporal shifting, or 4) poor ECMWF pressure fields. Unfortunately, most of the time, supporting data were not available to provide a specific reason. Consequently, the analysis is presented with suggestions of most likely candidates for the difference.

5. Results

In this study, we surveyed *ERS-1* swaths for coincidence with strong midlatitude storms. The *ERS-1* scatterometer is a polar-orbiting, sun-synchronous active radar. It has a 500-km-wide swath, with subsequent passes at an interval of about 90 min. Swaths are separated by a gap that depends on latitude, varying from 1000 km at 30° to 0 km at 70°. We have investigated

TABLE 1. Summary of cases.

Location	Date *ERS-1*/EC analysis time (UTC)	P_{scat} (mb)	P_{EC} (mb)
46°N, 160°E	23 Jan 1992 1200/1200	971	973
51°N, 165°E	5 Feb 1992 1130/1200	987	988
40°N, 142°W	8 Feb 1992 1900/1800	976	985
43°S, 112°W	11 Feb 1992 1630/1800	993	1010
37°N, 170°E	14 Feb 1992 1130/1200	970	971
38°N, 176°E	18 Feb 1992 1030/1200	983	985
46°S, 140°W	3 Mar 1992 0900/1200	989	990
53°N, 170°E*	3 Mar 1992 2300/0000**	976	980
20°S, 165°E	4 Mar 1992 1200/1200	996	996
48°N, 173°W	5 Mar 1992 2200/0000**	963	952
50°N, 171°W*	6 Mar 1992 0900/1200	972	972
53°S, 114°W*	6 Mar 1992 1700/1800	994	1000
49°S, 11°W*	4 Jul 1992 0900/1200	976	964
47°S, 71°E*	10 Jul 1992 1900/1800	972	978
48°S, 96°E*	11 Jul 1992 0200/0000	976	982
37°S, 30°W	22 Aug 1992 0120/0000	1006	1006
47°S, 40°E	23 Aug 1992 2100/1800	978	985
38°N, 139°W	26 Aug 1992 1800/1800	993	996
46°N, 35°W	5 Nov 1992 0040/0000	984	988
58°N, 172°E	12 Nov 1992 1000/1200	965	962
56°N, 144°W	14 Nov 1992 0800/0600	981	977
42°S, 17°W*	16 Nov 1992 1000/1200	982	987
47°S, 12°W*	17 Nov 1992 0900/0600	980	984
44°N, 45°W	12 Dec 1992 1330/1200	985	986
47°N, 153°E	14 Dec 1992 1200/1200	974	978

* The center of the cyclone is not included within the swath. The lowest scatterometer-retrieved pressure is compared to the ECMWF analysis at the same location.

** The UTC time for the next day.

the minimum pressures attained in 13 storms in the Northern Hemisphere midlatitudes and in 12 storms in the Southern Hemisphere. Table 1 shows information for all of the storms surveyed.

Because of the limited coverage of the *ERS-1* swath, it is difficult to obtain coincidence at synoptic times. When analysis times were within 2 h, we moved the scatterometer track so that the low centers coincided. At the maximum rate of change for the storms we surveyed, an error of up to 3 mb could result.

A representative *ERS-1* swath of surface winds is shown in Fig. 1. The C-band scatterometer penetrates clouds so that there are no dropouts throughout the storm. The wind vectors are given to within 50 km of land. The gradient winds for the neutrally stratified case would simply be 18° to the right of and 1.5 times greater than the surface winds. When stratification data are used in the PBL model, these factors would vary between 5° and 30° and between 1.2 and 2.3 (unstable–stable stratification). The net effect of the stratification correction on surface pressures is about ±2 mb. A similar magnitude correction sometimes resulted from thermal wind effects in the highly baroclinic regions around the storms.

The surface pressure fields for the winds in Fig. 1 are shown in Fig. 2. The scat/PBL pressures are restricted to the 500-km swath width. In this case, the *ERS-1* swath occurred at the synoptic time, and both analyses (model and ECMWF) gave a low pressure of 996 mb. There is characteristic agreement between isobar curvatures, although the model pressure fields may

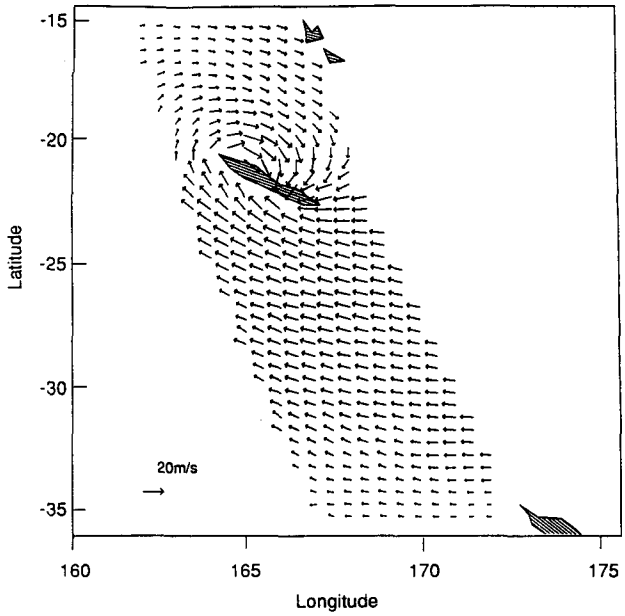

FIG. 1. *ERS-1* scatterometer wind (m s^{-1}) interpolated to a 0.5° × 0.5° grid (same interpolation is in Figs. 4a–8a) at 1200 UTC 4 March 1992.

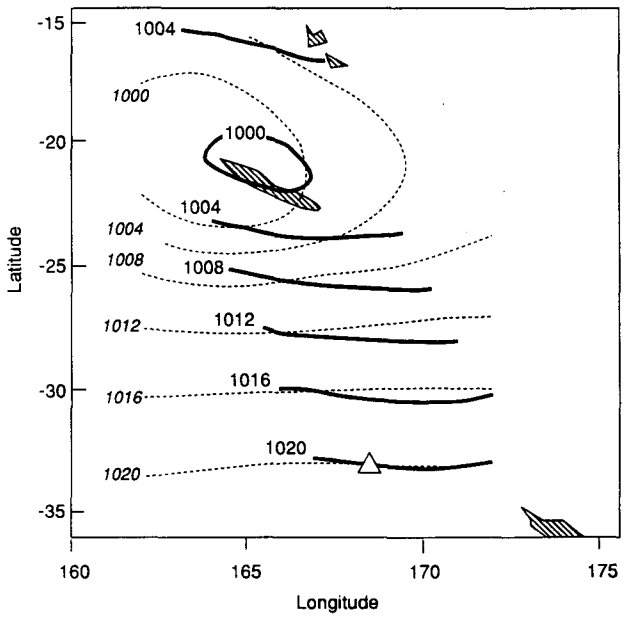

FIG. 2. Sea level pressures (mb) from scat/PBL winds (solid lines) and ECMWF (dashed lines) at 1200 UTC 4 March 1992. A triangle marks the reference point for the scat/PBL wind-derived pressure (same as in Figs. 4b–8b).

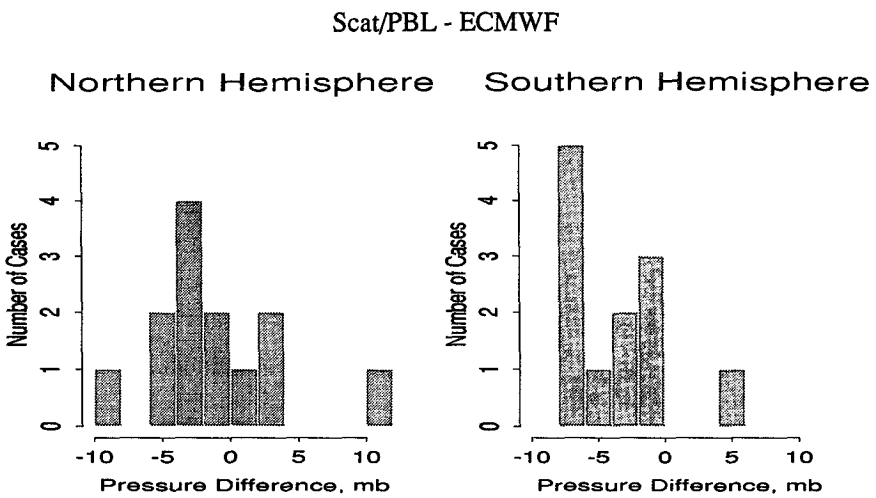

FIG. 3. Histogram of the difference between the scat/PBL and ECMWF sea level pressures for the storms surveyed.

show tendencies that are absent in the ECMWF analysis. These are assumed to be significant only when they are independent of grid spacing in the analysis. There is always incentive to maximize grid spacing in the scat/PBL model since computer demands are inversely proportional. *ERS-1* wind fields are available at 25-km intervals. For the purposes of this analysis, a 50-km grid was used, and the pressures were smoothed on a 100-km scale.

The histogram in Fig. 3 shows a summary of the central pressure differences for the storms studied. There is a marked difference in Northern–Southern Hemisphere agreement, apparently due to differences in the amount of data available to the numerical model. There are significant departures from the average differences that we will address individually.

Another example of good agreement between the analyses is shown in Fig. 4, regarding a North Pacific

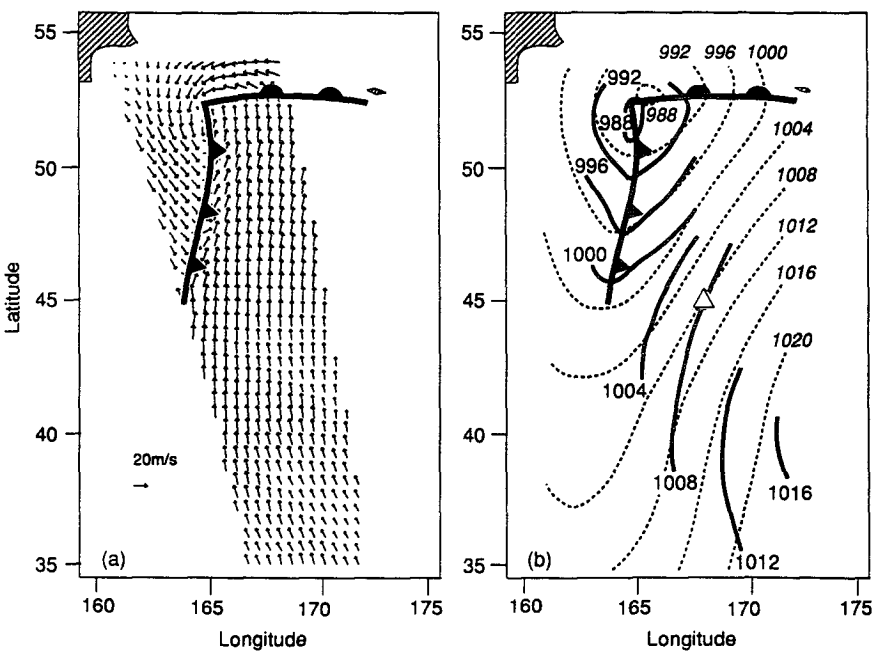

FIG. 4. (a) *ERS-1* scatterometer wind (m s^{-1}) at 1130 UTC 5 February 1992. (b) Sea level pressures (mb) from scat/PBL winds (solid lines) and ECMWF (dashed lines) at 1200 UTC (dashed line) on 5 February 1992.

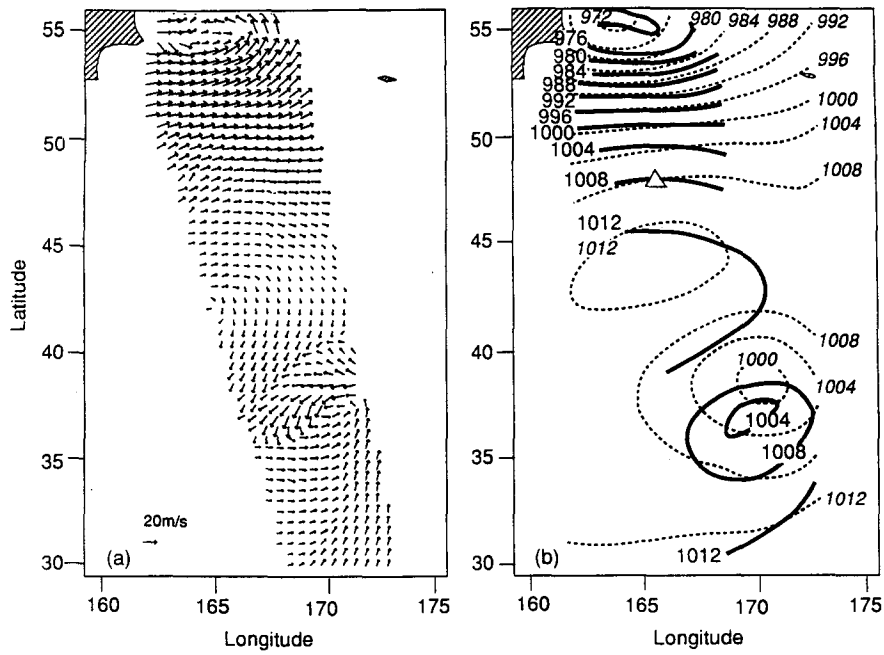

FIG. 5. (a) *ERS-1* scatterometer wind (m s^{-1}) at 1130 UTC 14 February 1992. (b) Sea level pressures (mb) from scat/PBL winds (solid lines) and ECMWF (dashed lines) at 1200 UTC (dashed line) on 14 February 1992.

storm. The scatterometer delineation of the front and the resulting sharp turn in the isobars is illustrated here. Figure 5 shows a complicated field in the same North Pacific area with two lows. The scat/PBL analysis is 3 mb lower in the northern storm and 4 mb higher in the southern storm.

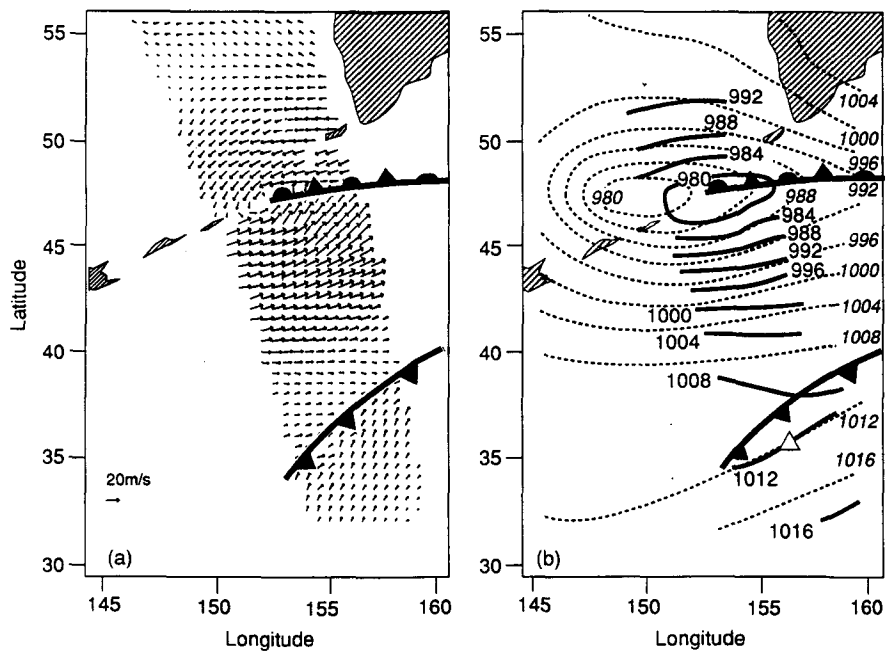

FIG. 6. (a) *ERS-1* scatterometer wind (m s^{-1}) at 1200 UTC 14 December 1992. (b) Sea level pressures (mb) from scat/PBL winds (solid lines) and ECMWF (dashed lines) at 1200 UTC (dashed line) on 14 December 1992.

An example of the details available in the wind field translated to pressure field is shown in Fig. 6 in the North Pacific region. The front is clearly indicated in the northeast corner of the low. The convergence in the south suggested by the ECMWF analysis is shown in the scat/PBL analysis. The trailing edge of the front that is shown in the scatterometer data is evident in a Japanese Geostationary Meteorological Satellite (GMS) IR picture (not shown). The two fields are coincident in time. The ECMWF low is 978 mb. The scat/PBL neutral low is 976 mb, or 978 mb with stratification corrections.

Figure 7 shows a storm in the northern Pacific that was unusual in that the scat/PBL wind analysis predicted a 10 mb greater central pressure than did the ECMWF analysis. There was a buoy pressure confirming both analyses at 976 mb, but none at lower values. There is no supporting evidence for the lower central pressure. This is a "worst case" comparison. From the wind field, there is a shear line that appears in the south, perhaps associated with a cold air comma cloud. Subsequent NMC analyses show this development (but higher central pressures in the main low). The reduced wind/pressure gradient in this region is shown in both analyses.

Most storms in the Southern Hemisphere were picked up by both analyses. However, the scat/PBL analysis was often more detailed and generally showed stronger storms. Figure 8 shows a Southern Hemisphere analysis where the storm was completely missed by the numerical analysis.

6. Conclusions

The minimum pressures derived from the scat/PBL model are generally very close to those of the ECMWF analyses. Overall, the scatterometer-derived lows averaged 2 mb lower than the ECMWF analyses. However, this could be separated into about −1 mb in the Northern Hemisphere and −3 mb in the Southern Hemisphere. There is no difference in data available to the neutral/barotropic scat/PBL analysis in the two hemispheres, whereas there is considerable difference in data available to the ECMWF analysis. This suggests that the agreement in the north means that both analyses are doing well (an average difference of less than 1 mb) and agree with surface observations. The larger differences in the Southern Hemisphere result from the lack of data for initializing the numerical model. We have also compared pressures with the NMC Nested Grid Model, which has comparable resolution, with similar results.

The outliers show that one or both of the analyses can produce erratic results. Some cases are obvious, such as that of Fig. 8. However, there are sometimes large differences in the Northern Hemisphere that suggest there is a random error source. It is difficult to credit this error to the scatterometer signal, as it is unaffected by clouds and insensitive to precipitation in the C-band wavelength. However, it is likely that a "pressure bogusing" scheme based on satellite cloud characteristics can inject a random error. It is our understanding that the numerical models sometimes

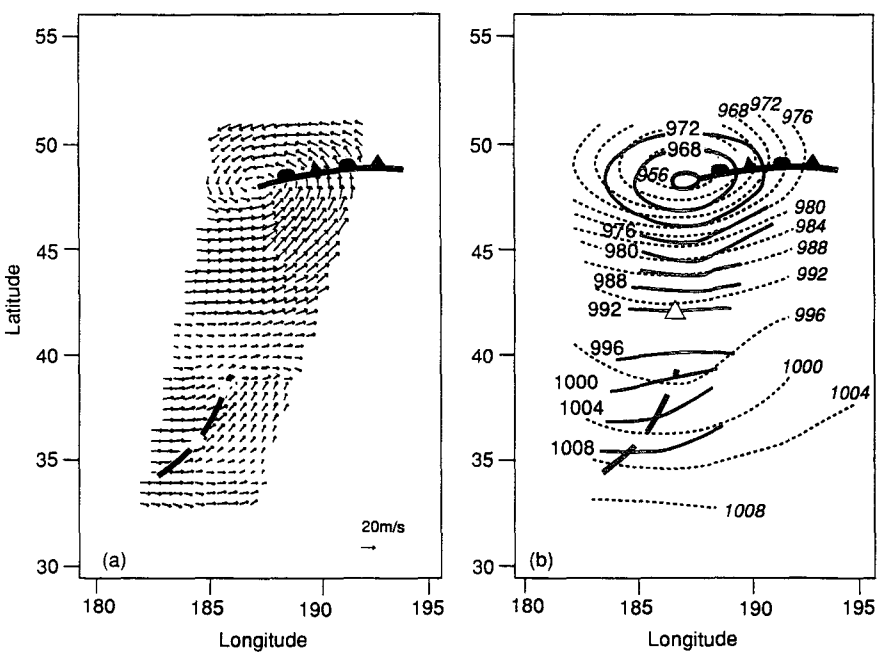

FIG. 7. (a) *ERS-1* scatterometer wind (m s^{-1}) at 2200 UTC 5 March 1992. (b) Sea level pressures (mb) from scat/PBL winds (solid lines) and ECMWF (dashed lines) at 0000 UTC 6 March 1992 (dashed line).

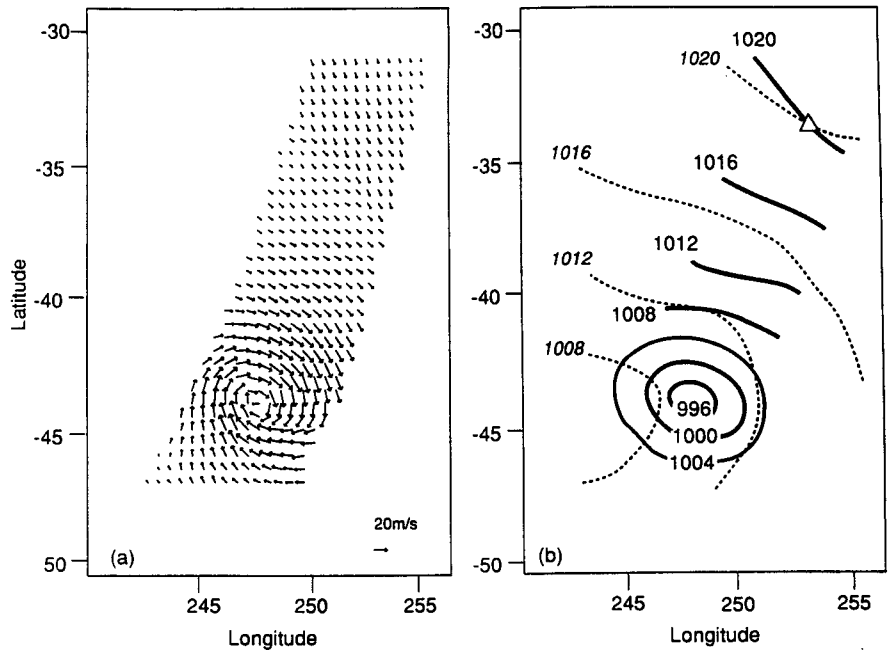

FIG. 8. (a) *ERS-1* scatterometer wind (m s^{-1}) at 1600 UTC 11 February 1992. (b) Sea level pressures (mb) from scat/PBL winds (solid lines) and ECMWF (dashed lines) at 1800 UTC 11 February 1992 (dashed line).

benefit from some ad hoc manipulation of the storm's pressures in order to obtain central values as low as those observed. While these pressure modification procedures may be qualitatively well based and successful, when scatterometer data can be used the pressures are more closely based on observations.

In general, the scat/PBL pressure fields agree well with ECMWF fields, with slightly lower pressures from the scat/PBL analysis. However, in one case the numerical analysis predicted a much lower pressure and in another case a much higher pressure, both of which were incompatible with observed wind fields.

There was a persistent difference in the two analyses with regard to the symmetry in the pressures around a storm core. Whereas ECMWF storm centers were consistently more symmetric, the scat/PBL analyses frequently have smaller pressure gradients on the high-latitude side. This can be seen in Fig. 6, where the *ERS-1* winds yield steeper gradients in the south of the storm and weaker gradients to the north. The asymmetry in the winds and pressures seen by the scat/PBL analysis is further developed when corrections for stratification and thermal wind are included.

The scatterometer winds represent observed, dense wind fields with errors comparable to those of ship and buoy reports. When translated into surface pressures, they represent one form of an observational reinitialization opportunity for the numerical forecast models. For example, Hoffman (1993) suggested that the scatterometer winds may be used more effectively in the mass field analysis when a synthetic surface pressure field is derived from them. The ramifications of deeper low pressures may be significant to neighboring analysis regions. The corresponding increased surface winds will have an effect on air–sea fluxes. This and other physical characteristics of the storms will become more evident with the accumulation of more scatterometer data.

Acknowledgments. This work was supported by the NASA Atmospheric Division and the NASA/JPL NSCAT/Seawinds Projects.

APPENDIX

Minimization of J

The expression of the cost function J is written in matrix form:

$$J = (\mathbf{Hx} - \mathbf{y})^{\mathrm{T}}\mathbf{R}(\mathbf{Hx} - \mathbf{y}),$$

where $\mathbf{x}$ is an N vector representing the surface pressure, $\mathbf{y}$ is a $2N$ vector representing the two components of $\mathbf{V}_{g1}$, and $\mathbf{H}$ is a $2N \times N$ matrix representing the finite-difference operation upon surface pressure to obtain the two components of $\mathbf{V}_g$. Here N is the total number of grid points with surface geostrophic wind, and $\mathbf{R}$ is a $2N \times 2N$ weight matrix. Superscript T stands for the transpose of a matrix. Since the *ERS-1* observation and the PBL model calculation are not considered to have spatial bias, $\mathbf{R}$ is diagonal with elements equal to 1.

To minimize J with respect to $\mathbf{x}$, we solve for $\mathbf{x}$ such that the following equations are satisfied:

$$\delta J = 2(\mathbf{Hx} - \mathbf{y})^{\mathrm{T}}\mathbf{RH}\delta\mathbf{x} = 0$$

or

$$(\mathbf{Hx} - \mathbf{y})^{\mathrm{T}}\mathbf{RH} = 0$$

or

$$\mathbf{H}^{\mathrm{T}}\mathbf{RHx} - \mathbf{H}^{\mathrm{T}}\mathbf{Ry} = 0.$$

The problem is now reduced to solving a linear system $\mathbf{Ax} = \mathbf{b}$, where $\mathbf{A} = \mathbf{H}^{\mathrm{T}}\mathbf{RH}$ and $\mathbf{b} = \mathbf{H}^{\mathrm{T}}\mathbf{Ry}$. The rank of $\mathbf{A}$ is $N - 1$. After one element in $\mathbf{x}$ is fixed, the remaining system, with dimension $N - 1$, is nonsingular, and a solution can be obtained. The conjugate gradient method is used to solve this linear system. The need to fix one element in $\mathbf{x}$ corresponds to the fact that a reference point of surface pressure has to be used to determine the value of the whole field.

REFERENCES

Anderson, R. K., et al., 1973: The use of satellite pictures in weather analysis and forecasting. WMO Tech. Note 124, 275 pp.

Brown, R. A., and W. T. Liu, 1982: An operational large-scale marine planetary boundary layer model. *J. Appl. Meteor.*, **21,** 261–269.

——, and G. Levy, 1986: Ocean surface pressure fields from satellite-sensed winds. *Mon. Wea. Rev.*, **114,** 2197–2206.

——, and R. C. Foster, 1994: On large-scale PBL modeling. *J. Atmos.–Ocean System,* in press.

Foster, R. C., and R. A. Brown, 1994: PBL modelling for GCMs: A comparison between a two-layer similarity and higher order closure model. *J. Atmos.–Ocean System,* in press.

Freilich, M., and R. S. Dunbar, 1992: A preliminary C-band scatterometer model function for the *ERS-1* AMI instrument. *Proc. First ERS-1 Symp.* Cannes, France, European Space Agency, 79–83.

Guymer, L. B., 1978: Operational application of satellite imagery to synoptic analysis in the Southern Hemisphere. Bureau of Meteorology Tech. Rep. 29, Melbourne, Australia, 83 pp.

Hoffman, R. N., 1993: A preliminary study of the impact of the *ERS-1* C band scatterometer wind data on the European Centre for Medium-Range Weather Forecasts global data assimilation system. *J. Geophys. Res.*, **98**(C6), 10 233–10 244.

Junker, N. W., and D. J. Haller, 1980: Estimation of pressure by satellite cloud pattern recognition. Preprints, *Eighth Conf. on Weather Forecasting and Analysis,* Denver, Amer. Meteor. Soc., 119–122.

Liu, W. T., K. B. Katsaros, and J. A. Businger, 1979: Bulk parameterization of air–sea exchanges of heat and water vapor including the molecular constraints at the interface. *J. Atmos. Sci.*, **36,** 1722–1735.

Smigielski, F. J., and H. M. Mogil, 1991: Use of satellite information for improved oceanic surface analysis. Preprints, *First Int. Symp. on Winter Storms,* New Orleans, Amer. Meteor. Soc., 137–144.